

Discharge and flow characterizations of the double-side sliding discharge plasma actuator

Qi-Kun He(贺启坤), Hua Liang(梁华), Bo-Rui Zheng(郑博睿)

Citation: Chin. Phys. B . 2020, 29(6): 064702 . **doi:** 10.1088/1674-1056/ab8624
Journal homepage: http://cpb.iphy.ac.cn; http://iopscience.iop.org/cpb

What follows is a list of articles you may be interested in

Dynamic evolution of vortex structures induced bytri-electrode plasma actuator

Bo-Rui Zheng(郑博睿), Ming Xue(薛明), Chang Ge(葛畅)

Chin. Phys. B . 2020, 29(2): 024704 . **doi:** 10.1088/1674-1056/ab671f

Aerodynamic actuation characteristics of radio-frequency discharge plasma and control of supersonic flow

Zhen Yang(杨臻), Hui-Min Song(宋慧敏), Hong-Yu Wang(王宏宇), Shan-Guang Guo(郭善广), Min Jia(贾敏), Kang Wang(王康)

Chin. Phys. B . 2019, 28(2): 024701 . **doi:** 10.1088/1674-1056/28/2/024701

Gas flow characteristics of argon inductively coupled plasma and advections of plasma species under incompressible and compressible flows

Shu-Xia Zhao(赵书霞), Zhao Feng(丰曌)

Chin. Phys. B . 2018, 27(12): 124701 . **doi:** 10.1088/1674-1056/27/12/124701

Numerical analysis of plasma arc physical characteristics under additional constraint of keyhole

Bin Xu(徐斌), Fan Jiang(蒋凡), Shujun Chen(陈树君), Manabu Tanaka(田中学), Shinichi Tashiro(田代真一), Nguyen Van Anh

Chin. Phys. B . 2018, 27(3): 034701 . **doi:** 10.1088/1674-1056/27/3/034701

Comparison between AlN and Al_2O_3 ceramics applied to barrier dielectric of plasma actuator

Dong-Liang Bian(卞栋梁), Yun Wu(吴云), Min Jia(贾敏), Chang-Bai Long(龙昌柏), Sheng-Bo Jiao(焦胜博)

Chin. Phys. B . 2017, 26(8): 084703 . **doi:** 10.1088/1674-1056/26/8/084703

Discharge and flow characterizations of the double-side sliding discharge plasma actuator*

Qi-Kun He(贺启坤)[1], Hua Liang(梁华)[1,†], and Bo-Rui Zheng(郑博睿)[2,‡]

[1] *Science and Technology on Plasma Dynamics Laboratory, Air Force Engineering University, Xi'an* 710038, *China*
[2] *School of Automation and Information, Xi'an University of Technology, Xi'an* 710048, *China*

(Received 30 December 2019; revised manuscript received 14 March 2020; accepted manuscript online 3 April 2020)

We investigate the discharge and flow characterizations of a double-side siding discharge plasma actuator driven by different polarities of direct current (DC) voltage. The discharge tests show that sliding discharge and extended discharge are filamentary discharge. The irregular current pulse of sliding discharge fluctuates obviously in the first half cycle, ultimately expands the discharge channel. The instantaneous power and average power consumptions of sliding discharge are larger than those of the extended discharge and dielectric barrier discharge (DBD). The flow characteristics measured by a high-frequency particle-image-velocimetry system together with high-speed schlieren technology show that the opposite jet at the bias DC electrode is induced by sliding discharge, which causes a bulge structure in the discharge channel. The bias DC electrode can deflect the direction of the induced jet, then modifying the properties of the boundary layer. Extended discharge can accelerate the velocity of the starting vortex, improving the horizontal velocity profile by 203%. The momentum growth caused by extended discharge has the largest peak value and the fastest growth rate, compared with sliding discharge and DBD. However, the momentum growth of sliding discharge lasts longer in the whole pulsed cycle, indicating that sliding discharge can also inject more momentum.

Keywords: plasma, double-side sliding discharge, induced velocity, induced vortex, momentum analysis

PACS: 47.32.C–, 47.65.Md, 52.30.–q, 52.50.Nr **DOI:** 10.1088/1674-1056/ab8624

1. Introduction

Plasma flow control is a burgeoning active flow control technology.[1] Roth from the University of Tennessee firstly used the one-atmospheric-pressure uniform glow discharge (OAUGDP) to research boundary layer control, airfoil separation and turbulence flow drag reduction.[2,3] Since then, many teams have carried out research on the aerodynamics of plasma technology. Plasma flow control is effective in controlling the boundary layer,[4,5] separation flow,[6–8] shear flow,[9] increase of drag reduction,[10] and plasma anti-icing.[11] Compared to conventional flow control technology, plasma flow control has no mechanical components, low energy consumption and fast response speed, and can use minor and local disturbances to achieve large-scale and global control.[12,13]

As the core component of plasma flow control, the performance and structure design of plasma actuators are the key to achieve flow control. The mostly conventional actuators currently are direct current (DC) corona discharge plasma actuators, plasma synthetic jet (PSJ) actuators and dielectric barrier discharge (DBD) plasma actuators. Among them, the dielectric barrier discharge plasma actuators could generate the low-temperature plasma by setting two parallel electrodes on both sides of the dielectric material. The charged particles, driven by electromagnetic field force, can induce and control the gas on the surface of the dielectric, and then apply aerodynamic actuation to the boundary layer.[2] Although the flow control form of DBD is effective in restraining stall separation, reducing flow resistance and suppressing aerodynamic noise, it still has some disadvantages such as small discharge area, insufficient intensity and uncontrollable direction of the induced jet, which all greatly restrict the development of plasma flow control.[14]

Further research has shown that two opposite jets can be induced by a symmetrical two-electrode DBD actuator. The vortex in the reverse direction can enhance the mixing ability of the flow field and inject more momentum. The jet in the same direction of the incoming flow can accelerate the airflow, and the vortex can enhance the mixing ability and accelerate the airflow simultaneously. On the other hand, in order to increase the interaction area, Moreau *et al.*[15] added another exposed electrode to the conventional DBD configuration, generating a tri-electrode sliding discharge plasma actuator. An unbalanced electric field is generated between the three electrodes. The flow visualization results showed that the flow characteristics were completely different from the typical DBD actuators. Therefore, to improve the induced airflow velocity and to increase the interaction area, a double-side sliding discharge plasma actuator (DSDPA) is adopted in the

*Project supported by the National Natural Science Foundation of China (Grant Nos. 51607188, 51790511, and 51906254) and the Foundation for Key Laboratories of National Defense Science and Technology of China (Grant No. 614220202011801).

†Corresponding author. E-mail: lianghua82702@126.com
‡Corresponding author. E-mail: narcker@163.com

© 2020 Chinese Physical Society and IOP Publishing Ltd

present study. Based on the symmetrical plasma actuation and the large-scale surface discharge driven by high DC voltage, DSDPA can enhance the body force, and generate two groups of unsymmetrical large-scale vortex coherent structures.[16] If the bias electrode is connected to a high negative DC voltage, plasma discharge will be enlarged significantly. In this case, the negative DC voltage could induce new vortices and jets to hinder the mainstream. Eventually the collision of two horizontal ionic winds with same intensity, and the opposite directions will form a new synthetic jet with a controllable direction.[15–17] The discharge filaments across the whole gap can be observed between high voltage electrode and the negative DC high voltage. This type of actuation is called sliding discharge.[18] When the bias electrode is connected to the positive DC voltage, the induced electrohydrodynamic (EHD) force would be enhanced. Additionally, the structure of the induced flow field could be strengthened.[19,20] The positive DC voltage has a little effect on the plasma region and this discharge morphology is similar to that of DBD, so that it is called extended discharge.[21]

Under a flight condition, the flow field around the nearly cylindrical missile or fighter jet head at a high angle of attack or even stall may show a complex multi-vortex structure, in which the flow characteristics rapidly change. Eventually the aerodynamics and moments become very unstable and nonlinear.[4,5] Due to the actuator's structure that could generate double-sided discharge, DSDPA can inject the EHD force on both sides of the actuator. The asymmetric vortex caused by DSDPA moves in the opposite direction through the pulling effect of the slender body. This effect can increase the distance between the cores of the asymmetric vortices, weaken the interaction, and increase the instability of the vortices.

Currently, sliding discharge and expanded discharge are mainly researched with the geometry of tri-electrode structure. Louste *et al.*[22] set an exposed electrode driven by high DC voltage in parallel. This structure is capable of forming sliding discharge between two exposed electrodes under the actuation of a negative DC high voltage. Using the schlieren system, Moreau *et al.*[23] conducted an experimental study on electric wind of surface discharge by adopting the mode of alternating current (AC) and DC high voltage. It was found that the structure of the induced flow field could be significantly changed, and it was observed that changing DC voltage could increase the maximum induced velocity by 150%, but the evolution mechanism of the flow field was not elaborated. Guo *et al.*[24] adjusted the above actuators. They connected two electrodes on the upper surface of the dielectric material with the high-voltage diode and the high-voltage power. A layer of hydrogenated amorphous silicon is filmed on the surface of the dielectric material. Experimental results showed that the structure of the actuator could increase the thrust by 70% compared with the traditional actuator. We previously analyzed the rules of formation, evolution and interaction with $t^* < 0.1$, and further explained the flow and electric characteristics of sliding discharge induced by a double-side sliding plasma actuator.[17,25] Pang *et al.*[26,27] concentrated on the differences of the characteristics of the discharge generated by positive pulses and negative pulses, and discussed the underlying physical mechanism by researching the effect of electrode width and the gap distance on the plasma morphology. Bayoda *et al.*[28] indicated that this drift is affected by the excitation voltage, whereas the propagation speed of the discharge increases with the amplitude of the negative DC component. For sliding discharge, the pressure wave consists of two circular waves located over the two upper electrodes. Researchers also paid attention to the three-electrode geometry excited by a nanosecond pulse and a DC source, finding that the negative DC voltage can induce a weak circular pressure wave.[29,30]

To explore the formation mechanism of the induced flow field of DSDPA and to display the spatial-temporal evolution of the induced flow field, it is necessary to adopt high-time flow field observation technology. In this paper, synchronous actuation is applied on a DSDPA driven by different polarities of DC high voltage. The high-frequency particle-image-velocimetry (PIV) technology and high-speed schlieren display technology are used to display the timing characteristics and structure of the flow field under static atmosphere. This work aims at improving the theoretical basis of flow control technology and providing necessary flow field data for the establishment of thrust enhancement studies.

2. Experimental equipment and system

The experimental equipment and system was mainly composed of a plasma actuation system, a high-speed schlieren system and a high-speed phase-locked PIV system.

2.1. Plasma actuation system

2.1.1. Plate electrode configuration

The structure of a double-side sliding discharge plasma actuator is shown in Fig. 1. The experiment was carried out in ambient air environment.

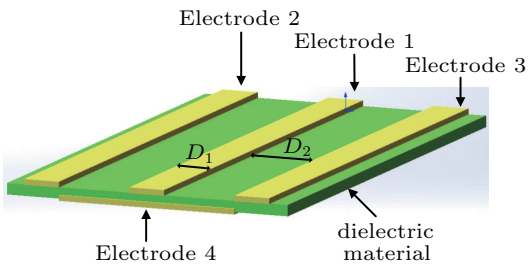


Fig. 1. Structure diagram of double-side sliding discharge plasma actuator.

The insulating dielectric material is polytetrafluoroethylene with the thickness 1 mm and the dielectric constant 2.17. Different electrodes are parallel distributed on the surface of the dielectric material. On the upper surface, all of the electrodes were made of copper foil. The central electrode is electrode 1, connected to the alternating current pulse power supply. The left electrode is electrode 2, and the right electrode is electrode 3. Electrodes 2 and 3 are respectively connected to the DC high-voltage power supply. The dimensions of electrodes 1, 2 and 3 were 100 mm $\times$5 mm $\times$0.018 mm (D_1 = 5 mm). The distances between them were both 20 mm streamwise (D_2 = 20 mm). On the lower surface of the dielectric material, the package electrode is defined as electrode 4. The dimensions of electrode 4 was 120 mm $\times$45 mm $\times$0.018 mm.

2.1.2. Excitation power supply and discharge parameters test system

The pulse power supply of CTP-2000 K was used for discharge. The carrier frequency was fixed at 11 kHz. The pulse frequency was fixed at 5 Hz. The duty cycle could range from 1% to 100%, and the maximum power is 1000 W. The voltage U_{AC} was measured by using a high voltage probe of Tektronix P6015A, and the current I_1, I_2, I_3 were measured by using the current probe of TCP0030A. The electrical signals of the voltage and current were recorded by an oscilloscope of Tektronix DPO4104B (1 GHz bandwidth, sampling rate 5 GS/s). In our test, the duty ratio was 50% for the analysis of the unsteady flow.

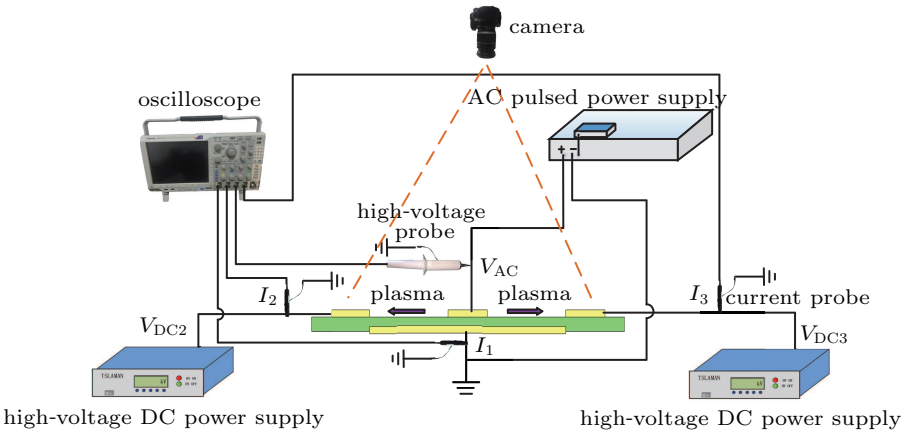


Fig. 2. Experimental setup and measurement system.

2.2. High-speed schlieren system

The experimental system consists of the following components: light source (xenon lamp), a pair of convex lenses, a pair of plane mirrors, a pair of spherical mirrors, and a knife edge. The image is taken by a PCO-Dimax HS1 high-speed camera with a resolution of 1000 $\times$ 1000. The maximum image capture rate can reach 180000 fps. In my experiments, the shooting rate is 22735 fps, the resolution is 502 $\times$ 402, and the system layout is shown in Fig. 3. The experimental temperature was 15 ℃ and atmospheric pressure was 1×10^5 Pa.

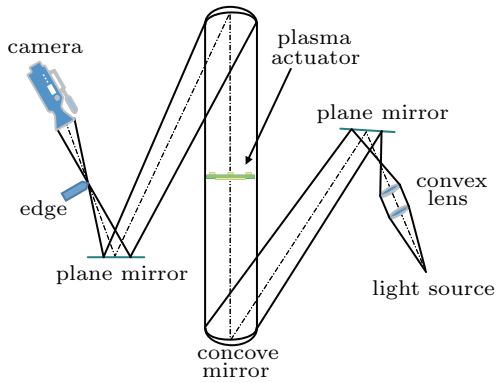


Fig. 3. High-speed schlieren system.

2.3. High-speed phase-locked particle image velocimetry system

The high-speed phase-locked PIV system consists of the following components: high-frequency laser (Photonics Industries DM series laser), high speed camera (Phantom V711) with an image resolution of 1280 $\times$ 800 and the maximum acquisition rate of 7500 Hz, programmable timing unit (La Vision), smoke generator, computing platform, and image post-processing software (Davis7.0).

The axis of the high-speed camera is perpendicular to the laser plane with an appropriate distance to ensure the adjustable shooting field and focal length. A resin glass cover is employed to ensure the stability of the flow field. In the experiment, the capturing frequency is 1000 Hz. Ultimately the instantaneous flow field can be obtained by time-averaged processing of PIV data at the same phase. The layout of the velocity-measuring system is shown in Fig. 4.

By using the Dynamic Studio software for cross-correlation processing, the flow field velocity vector distribution results are obtained. The diagnostic window is 32 pixels $\times$32 pixels, and the overlap ratio is 75%. In order to ensure the two-dimensional characters of the flow field, the strongest

position of the laser beam is set at 50% of the electrode. The plane of the laser beam is perpendicular to the exhibition of the electrode. The camera shooting area is 105 mm ×63 mm. The time interval between the two laser pulses is 100–300 μs. The total acquisition time is 1 s. The calculation results are based on the initial data collected by PIV, and no filtering and smoothing were performed.

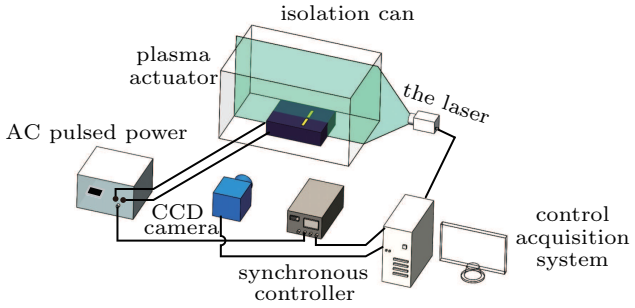


Fig. 4. Layout chart of high-speed PIV system.

3. Experimental results and analysis

3.1. Electrical characteristic analysis for DSDPA

3.1.1. Voltage and current characteristic analysis for DSDPA

The discharge images of DSDPA under different polarities of DC voltage were observed and compared. The experiments focused on the effects of different polarities of DC voltage and tried to research the advantages of sliding discharge and extended discharge compared with DBD in discharge and flow characteristics, so the current experiments did not apply DC voltage to electrode 3. However it is necessary for electrodes 1 and 3 to be both connected by the DC high-voltage power supply. The actuation parameters and modes are listed in Table 1.

Table 1. Test conditions for DSNP plasma actuator discharge characteristics.

	Electrode 1 U_{DC}	Electrode 2 U_{AC}	Electrode 3 U_{DC}
Case 1	0 kV	13 kV	0 kV
Case 2	−8 kV	13 kV	0 kV
Case 3	+8 kV	13 kV	0 kV

Different polarities of DC voltage were applied to electrode 1. The voltage and current waveforms were synchronously collected through the oscilloscope while the discharge images were taken. The discharge images obtained are shown in Fig. 5.

The exposure time of the discharge image is 1/160 s, and ISO is set at 4000. There is a threshold voltage ($U_{AC,t}$ = 3.72 kV in the experimental state) for the generation of plasma, and a threshold voltage of 5.22 kV is also required for DC voltage applied to electrode 1 for sliding discharge. Driven by the DC high voltage of −8 kV, the discharge intensity is same as DBD. The ion drift is generated at electrode 1 and extends along the interval of electrode 2 driven by the negative DC voltage, ultimately forming the discharge channel filled with discharge filaments. The discharge intensity is distributed uniformly in this channel, indicating that sliding discharge occurs under the drive of the negative DC voltage. Meanwhile, a "spot" with uneven luminance was observed at the edge of electrode 1. The discharge filaments concentrated at the spot, leading to high luminous intensity. Under the actuation condition of case 3, there are no luminescence and discharge filaments at electrode 2 driven by a positive DC voltage, and there is no significant difference in discharge intensity on both sides of electrode 1. This discharge mode is called expanded discharge.[19]

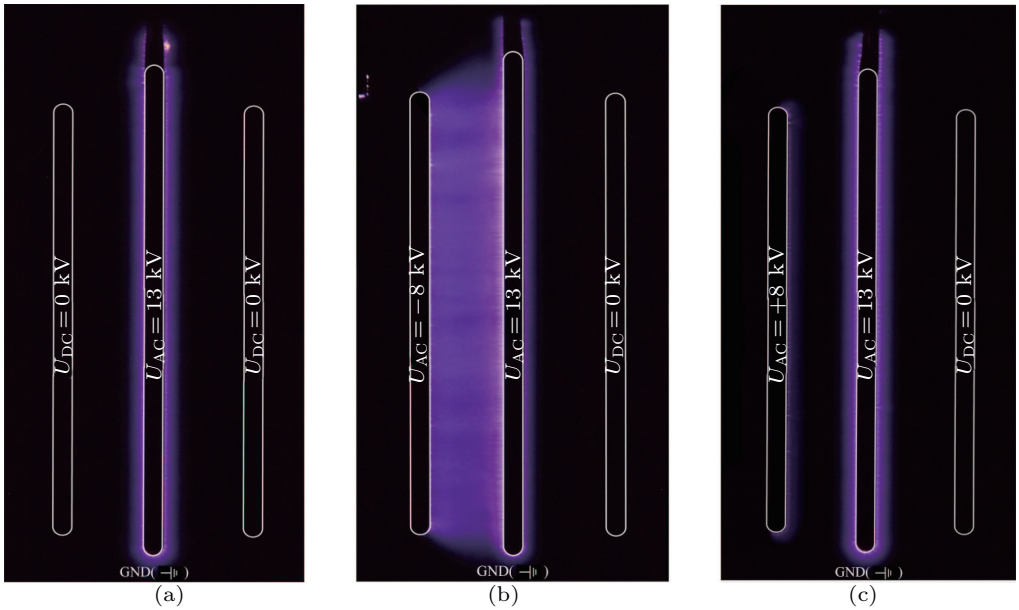


Fig. 5. Discharge diagrams of DSDPA under different DC voltages: (a) $U_{DC} = 0$ kV, (b) $U_{DC} = -8$ kV, (c) $U_{DC} = +8$ kV.

Further, the uniformity of dielectric barrier discharge can be accurately judged by measuring the voltage-current waveform. In the filamentary discharge, the current waveform has several current spikes of the nanosecond level in every half cycle of the sinusoidal waveform, while only a single or multiple long current pulses discernable in the field of view could be observed in the uniform discharge.[31]

In Fig. 6, during the first half cycle, the irregular current pulses fluctuate significantly, and a few of the discharge pulses have extremely high pulse peaks. Under different polarities of DC voltage, a large number of tiny irregular current pulses appear in the interval of 0.024 ms, which are caused by the ions drift to the downstream under the action of the EHD force.[32] The number of current spikes driven by the negative DC voltage is significantly greater than that of no DC and positive DC conditions. The maximum value is 3526 mA under the negative DC condition, the maximum value is 1587 mA under no DC condition, and the maximum value is 2084 mA under the positive DC condition. During the second half cycle, the current spike driven by the negative DC voltage is significantly less than that under no DC and positive DC conditions.

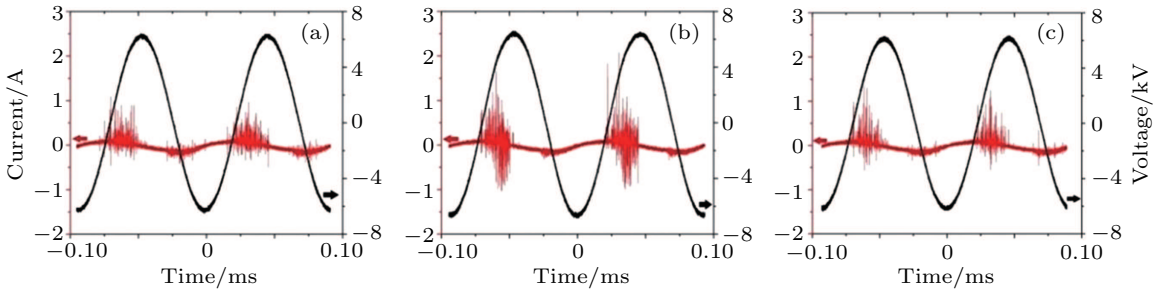


Fig. 6. Voltage-current waveform of DSDPA under different bias voltages: (a) $U_{DC} = 0$ kV, (b) $U_{DC} = -8$ kV, and (c) $U_{DC} = +8$ kV.

The above phenomena indicate that the discharge under different polarities of DC voltage is filamentary discharge. The short time multi-pulse characteristics of the current in each half cycle reflect the irregular intermittent advance of charge between the electrodes of the actuator. The charge accumulates on the surface of the dielectric material and generates an additional electric field opposite to the applied electric field. The superposition of the additional electric field and the applied electric field causes the intensity of the total electric field decrease, which is manifested as multiple steps of charge in every half cycle. Moreau *et al.*[23] found sliding discharge mode during one fraction of the positive AC cycle in which the voltage difference between electrodes enables the ignition of sliding discharge. In particular, the total current differs from the capacitive current (such as DBD current, see Fig. 6(b)).

According to the streamer theory,[33] under the influence of the applied electric field, the electron avalanche develops and rapidly moves towards the positive electrode. The additional electric field changes and superposes with the external electric field, resulting in distortion of the total electric field. The distorted total electric field further promotes the development of electron avalanche and produces a large quantity of photoionization and a secondary electron avalanche. The secondary electron avalanche will also move towards the positive electrode and superpose with the main electron avalanche to produce a streamer discharge area. Different from the traditional DBD, the driving of the DC high voltage interferes with the applied electric field and changes the field intensity in the interval. In the first half cycle of sinusoidal waveform, the existence of negative DC voltage increases the field intensity in the gas gap. The negative DC voltage accelerates the drift of the positive ions and the development of electron avalanche, thus forming a stable and uniform large area of low-temperature plasma in the whole electrode interval.[29] However, under the action of positive DC voltage, due to the fact that positive ions play a major role in the charge drift, no stable sliding discharge zone can be formed in the electrode interval.

3.1.2. Energy consumption analysis for DSDPA

In order to analyze the discharge energy under different polarities of DC voltage, the instantaneous power in the single cycle of the sinusoidal waveform was studied. The energy consumption for DSDPA was the superposition of the energy consumption driven by the AC pulse power supply and that driven by the DC high-voltage power supply. Here, the total power and energy consumption of DSDPA were calculated feasibly by the voltage and current of each electrode participating in the discharge. The following formula was used to calculate the instantaneous power of a single cycle:

$$P_t = U_{DC1}(t) \times I_1(t) + U_{DC3}(t) \times I_3(t) + U_{AC}(t) \times I_2(t). \quad (1)$$

The mean of the single cycle power of the AC voltage:

$$P = \frac{1}{T} \int_0^T P_t \mathrm{d}t. \quad (2)$$

The current I_1, I_2, I_3 were measured by the current probe and the voltage U_{AC} was measured by the high voltage probe in the discharge parameters test system. Figure 7 shows the instantaneous power consumption of DSDPA over a single cycle at different polarities of DC voltage.

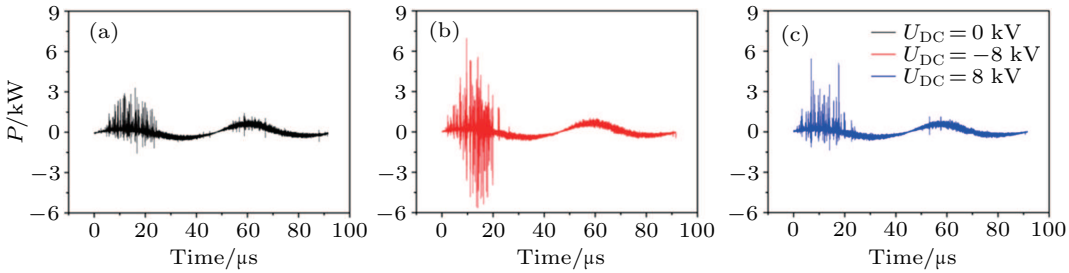


Fig. 7. Single-cycle instantaneous power of DSDPA under different polarities of DC voltage: (a) $U_{DC} = 0$ kV, (b) $U_{DC} = -8$ kV, (c) $U_{DC} = +8$ kV.

It can be seen that the instantaneous power of different kinds of discharge driven by AC voltage is mainly concentrated in the first half cycle of the sinusoidal waveform, which is the main area where the plasma is generated. When sliding discharge occurs, the discharge current pulses increase more than that of single DBD discharge. Kong *et al.*[29] revealed that the negative DC voltage can make the electric field intensity increase, resulting in the acceleration of ion drift towards the bias DC electrode, and thus, the fluid is significantly accelerated. This ion drift causes a heat release recombination process in the bias DC electrode and could induce interacting aerodynamic effects.

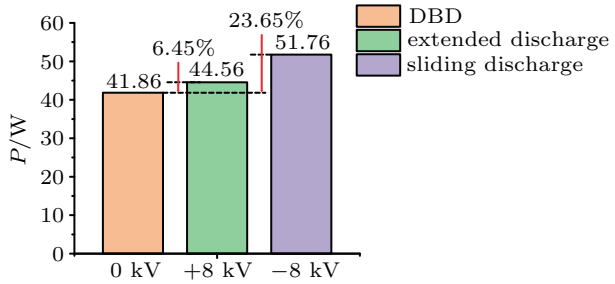


Fig. 8. Average power consumption of DSDPA under different polarities of DC voltage.

Further research is needed on the average power consumption. The average power of a single cycle is 51.8 W at −8 kV DC voltage, 41.8 W at no voltage, and 44.6 W at +8 kV DC voltage. The instantaneous power and average power consumption of sliding discharge are larger than that of extended discharge and DBD. Bayoda *et al.*[28] indicated that sliding discharge greatly increases the discharge energy deposited on the surface of the medium. Researchers also found a significant addition during the formation of sliding discharge, and clarified that the addition of power consumption is mainly due to the current pluses.[34]

3.2. The characteristics of flow field induced by DSDPA

Due to the different polarities of DC voltage, slide discharge and extended discharge occur in the double-side sliding discharge plasma actuator. The mode of the induced flow field changes fundamentally. The timing characteristics and structure of the induced flow under the positive and negative DC voltage are analyzed in the following.

3.2.1. The characteristics of induced flow field under negative DC voltage actuation

The actuation mode in case 2 was adopted, and the pulsed frequency was 5 Hz. The left side of the actuator was driven by a negative DC high voltage, forming discharge filaments across the entire electrode interval, known as sliding discharge.[18] A high-frequency PIV system and a high-speed schlieren system were employed to film the evolution of the flow field. In the image, the high-voltage electrode (electrode 1) of DSDPA is located at $x = 0$ mm, and the bias DC electrodes are located at $\Delta x = 20$ mm (electrode 2 is located at $x = -20$ mm, electrode 3 is located at $x = 20$ mm). The PIV results and schlieren diagrams from the start of the actuation to 0.1 T are analyzed in Fig. 8.

It can be observed that at the initial stage of discharge, the central electrode generated jet under the action of high voltage alternating current, which induced the starting vortex on both sides in Fig. 9(a). The generation of the induced vortex can be clearly seen in the PIV diagram and the schlieren image at the time of 5 ms. Meanwhile, the opposite jet under the negative DC high voltage is induced by electrode 2 against the high voltage electrode. The starting vortex and the opposite jet move towards each other, and finally collide in the electrode interval, causing the airflow movement to deflect.

The PIV diagrams in Figs. 9(c) and 9(d) show that the starting vortex of sliding discharge increases more slowly than that of DBD. Although electrode 1 continuously injects the EHD force to both sides, the opposite movement of the opposite jet hinders the horizontal movement of the starting vortex, and the momentum exchange also accelerates the starting vortex caused by the collision of the starting vortex and the opposite jet.

Further, the PIV diagram of the induced flow field at 15 ms was selected and the horizontal velocity profiles at different positions were analyzed.

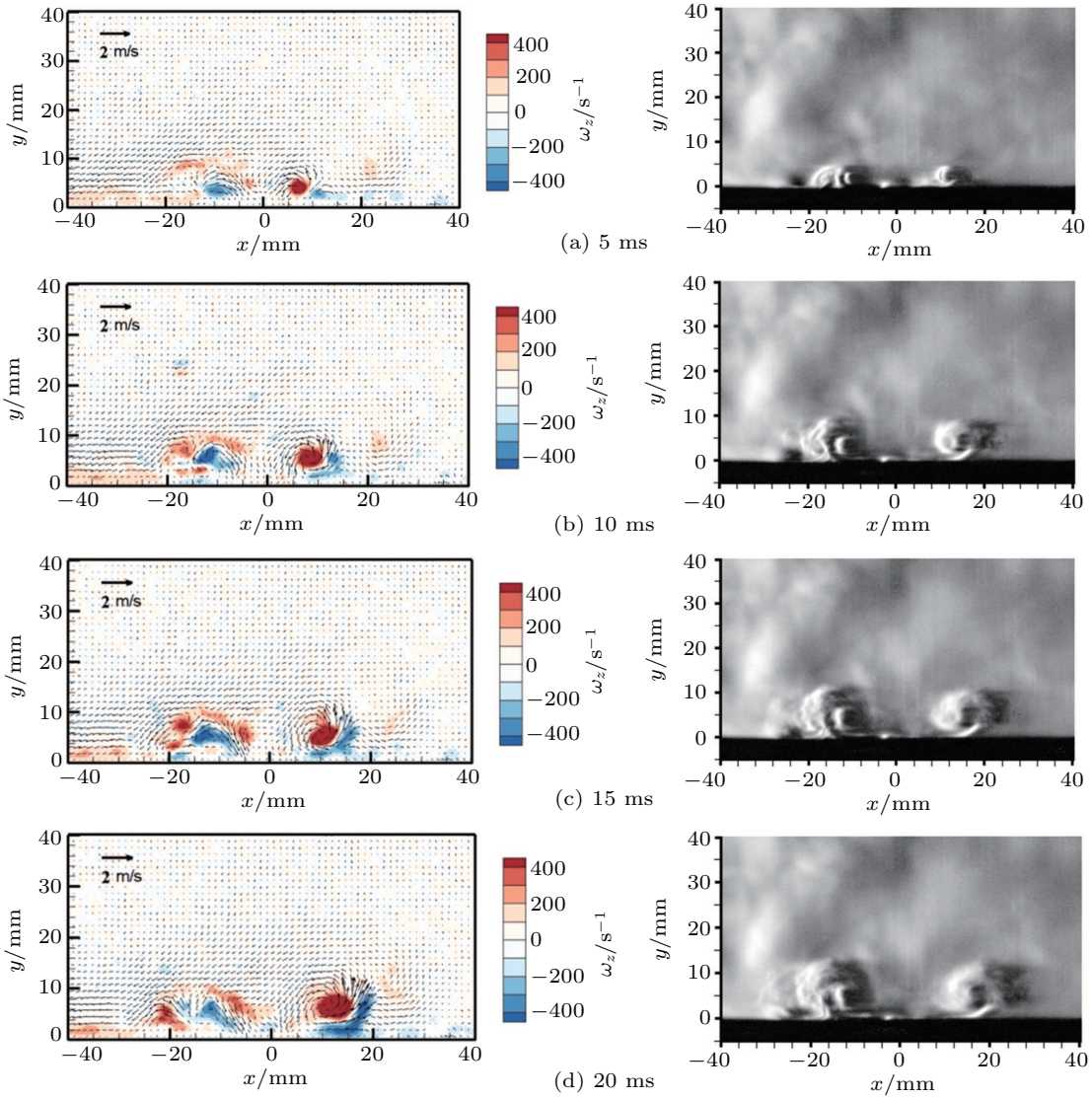


Fig. 9. PIV diagram and schlieren diagram of the flow field in sliding discharge at (a) 5 ms, (b) 10 ms, (c) 15 ms, and (d) 20 ms.

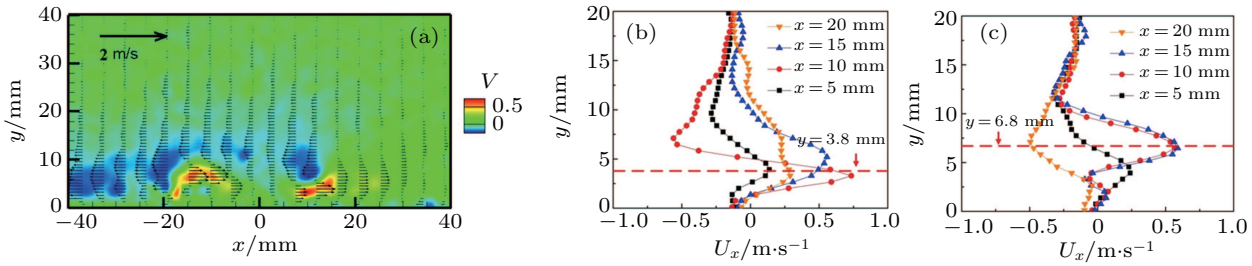


Fig. 10. The velocity profiles of case 2 at 15 ms: (a) the velocity profiles induced by the high-voltage bias electrode and the none-voltage bias electrode, (b) sliding discharge, (c) DBD.

Under the same actuated condition, the starting vortex is simultaneously induced on electrode 1. The velocity profiles at the $x = 5$ mm and $x = -5$ mm are symmetrically distributed. However, at $x = -10$ mm and $x = -15$ mm, the horizontal velocity profiles induced by electrode 2 is towards to the right, indicating that the opposite jet exerts additional disturbance to the flow field, and the disturbance of the opposite jet mainly occurs in the region of the electrode interval. The presence of a negative DC voltage on the left side attracts positive ions to drift toward electrode 1, while secondary electron emission also occurs on the surface of the bias electrode and produces negative ions. The drift of the negative ions under the EHD force produces a negative EHD force at the bias electrode, which appears as an induced jet emerging from the side of the bias electrode. Due to the presence of the opposite jet, the horizontal movement of the starting vortex is hindered, so that the horizontal velocity profile at the positions of $\Delta x = 10$ mm and $\Delta x = 15$ mm is biased to right. The momentum change

between the starting vortex and the opposite jet also slows the growth of the starting vortex driven by electrode 1. The peak value of the velocity profile in sliding discharge is basically located at the height of $y = 6.8$ mm. It is much higher than the peak value of DBD, which is basically located at the height of $y = 3.8$ mm. The jet changes the evolution of the velocity profile. At the same time, the height of the jet is also increased.

The collision between the starting vortex and the opposite jet caused the flow field to deflect.[16] With the voltage of electrode 2 increasing, the angle of the deflection was further increased. When the DC voltage was −10 kV, the induced flow field was vertically upward. The above results indicate that the existence of electrode 2 can deflect the direction of the flow field. It is helpful for the actuator to apply directional disturbance to the external flow field. The aerodynamic characteristics of the flow field provide methods to improving the ability of flow control and improving efficiency.

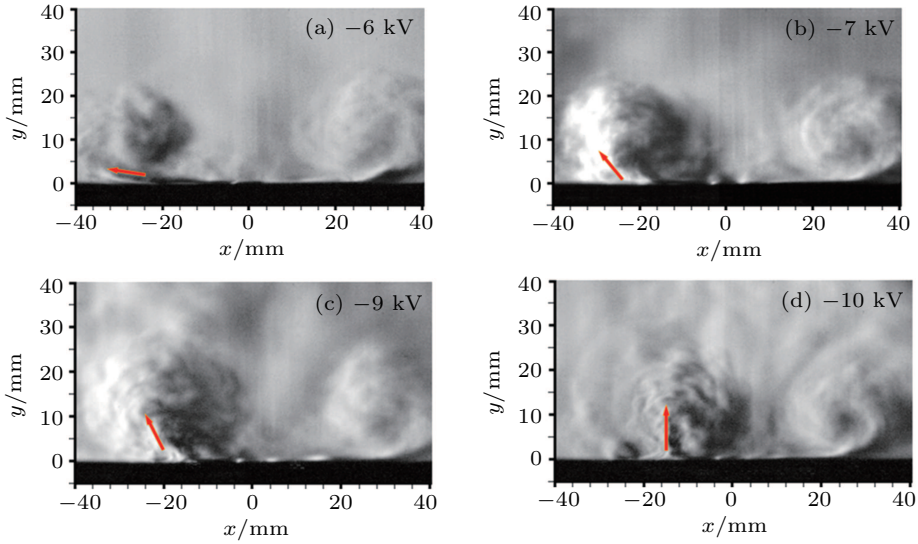


Fig. 11. High-speed schlieren diagram of flow field of sliding discharge under different DC voltages at $0.2T$.

3.2.2. The characteristics of induced flow field under positive DC voltage actuation

The actuation mode in case 3 was adopted, and the left side of the actuator was driven by a positive DC high voltage to generate extended discharge.[21] The dynamic evolution process of the starting vortex was observed by the high-speed PIV system, and the detailed evolution of the flow field from the start of the actuation to $0.1T$ was analyzed. The PIV results and schlieren diagrams of the flow field are shown in Fig. 12.

The pulsed discharge under the duty ratio makes the induced flow field unsteady. In Fig. 12(a), electrode 1 generated the EHD force, and two starting vortexes moved away from electrode 1. It can be clearly observed that under the plasma actuation, the starting vortex gradually spreads under the viscous dissipation with the effect of atmosphere damping. The horizontal velocity profile of the starting vortex in extended discharge is obviously faster than that in DBD discharge. It can also be known that extended discharge has a larger disturbance range in the horizontal direction.[35] The vortex promotes momentum mixing with the boundary layer more efficiently and the airflow moves closer to the dielectric surface, which is important for the jet acceleration.[30] Therefore, extended discharge shows the better potential ability for flow control.

Figure 13 shows the evolution of the horizontal velocity profile of extended discharge and DBD at three different positions of $\Delta x = 15$ mm, 25 mm, and 35 mm at the time of $0.1T$. The bias electrode is set at the position of $x = 20$ mm and $x = -20$ mm. There are similar horizontal velocities on the left and right sides at the position of $x = 15$ mm and $x = -15$ mm. However, at the position of $x = 25$ mm, the horizontal velocity profile of DBD starts to decrease and the maximum velocity decreases to about 0.4 m/s, while the horizontal velocity profile of extended discharge on the left side further increases to 0.95 m/s at the position of $x = -25$ mm. At the position of $\Delta x = 35$ mm, the horizontal velocity profile in extended discharge increases to 1.9 m/s, while there is barely any transverse velocity in DBD at the position of $x = 35$ mm. Zheng *et al.*[17] noted that plasma discharge can cause ions to abnormally accumulate on the bias electrode, which can result in the formation of a secondary electric field, weakening the primary electric field and reducing the synthetic electric field on the surface of the actuator. This phenomenon induces ions to increase the horizontal velocity profile. According to the evolution at the position $\Delta x = 35$ mm, the induced velocities firstly increase and secondly decrease during the period of $0.1T$, which reaches the maximum value at 15 ms. Especially, the maximum of the induced velocity at different moments changes basically at the same height.

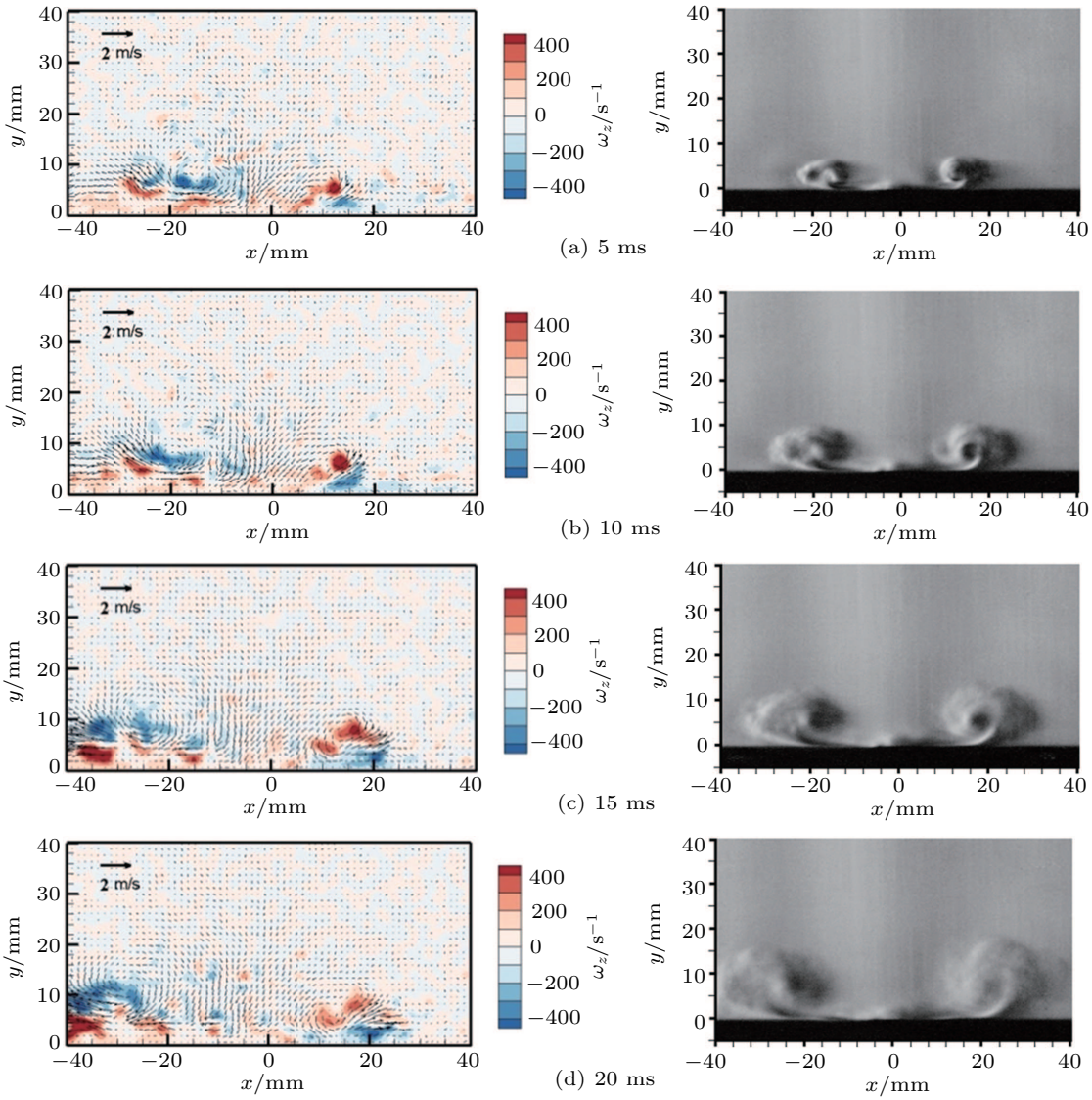


Fig. 12. PIV diagram and schlieren diagram of the flow field in the expanded discharge at 5 ms, 10 ms, 15 ms, and 20 ms.

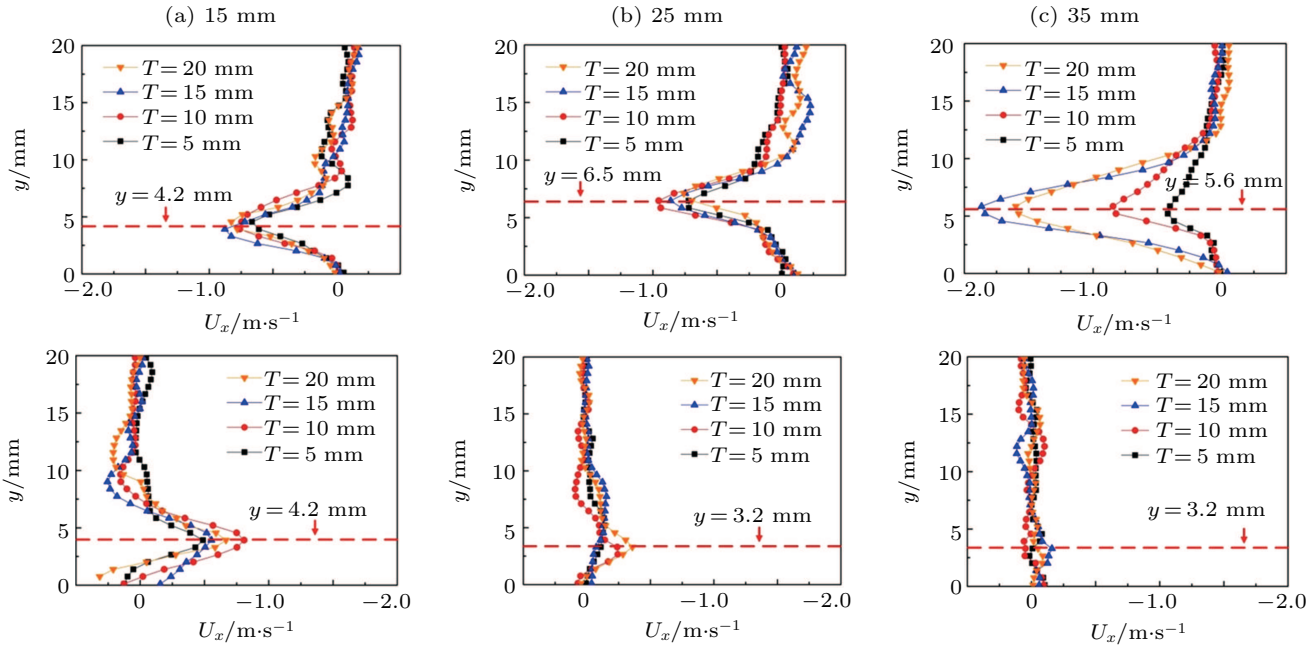


Fig. 13. Evolution of velocity horizontal component in three different positions of $\Delta x = 15$ mm, 25 mm, and 35 mm within the period of $0.1T$.

The plasma discharge has a significant acceleration effect on the nearby boundary layer. Compared with the traditional dielectric barrier discharge, extended discharge has larger area and larger intensity, which accelerates the growth of the vorticity.

The results of Soloviev's research[36] showed that the EHD force of AC-DBD is mainly caused by the second half cycle of the sinusoidal waveform, and the origin of the EHD force is the accumulation of the negative volume charge carried by the long-life O_2^- and O_3^-. The simulation by Nishida[37] on the tri-electrode actuator indicated that there is the negative EHD force on the bias electrode. Driven by the positive DC high voltage, the electrons triggered ionization to produce more positive ions. The drift motion of the positive ions under the EHD force produces the EHD force.

3.2.3. Comparison of induced velocity of extended discharge in different positions

The comparison of induced horizontal velocity between DBD and extended discharge showed that the induced velocity of extended discharge obviously increased. According to the velocity evolution, the velocities induced by extended discharge and DBD are equivalent within the range of $x = 0$–20 mm and $x = -20$–0 mm. In the range of $\Delta x = 20$–40 mm, the flow field induced by DBD gradually disappear under the action of air damping. The velocity induced by extended discharge is further increased under the action of the bias electrode, and reaches the maximum of $V_{x,\max} = 2.27$ m/s at the position of $x = -35$ mm.

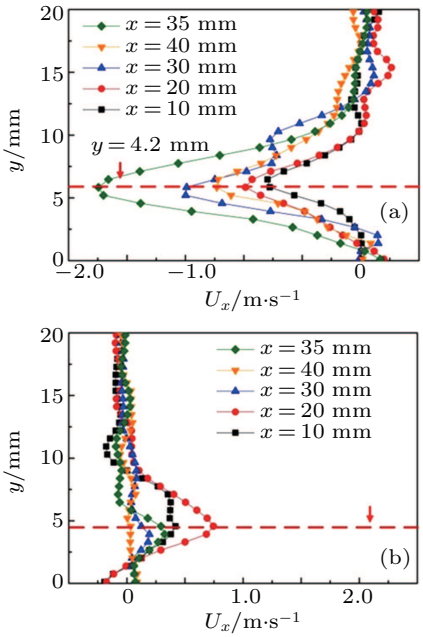


Fig. 14. Horizontal component of flow field velocity at five different positions of $\Delta x = 10$ mm, 20 mm, 30 mm, 35 mm, and 40 mm at $0.15T$.

In general, due to the existence of positive DC high voltage, the fluid element is accelerated at the bias electrode, increasing the induced velocity up to 203%. Nakai[38] analyzed the mechanism of the positive EHD force generation around the bias electrode and the negative EHD force generation around the central electrode. The drift motion of positive ions in extended discharge generates the positive EHD force around the bias electrode. The positive EHD force is enhanced by negative discharge which appears in the negative-going voltage phase of AC voltage because extended discharge is enhanced by supply of high density electrons from the negative discharge. The negative EHD force generation around the central electrode is largely contributed by the drift motion of negative ions generated by negative discharge. Therefore the unequal energy is injected in the double-side of DSDPA, which is the reason for inducing asymmetric vortices with different velocities and different vortex strengths.

3.3. Momentum analysis of DSDPA

Applying DC voltages with different polarities significantly changes the flow state of the induced flow field, which is due to the volumetric force on the side of the bias electrode. The EHD force is too small to measure. Within one pulsed period, the injection of energy is a mutative process. Therefore, by integrating the horizontal velocity profile on the PIV diagram of each moment, the flow momentum M_x in the x direction induced by DBD, extended discharge and sliding discharge is obtained.

The control body is set as $x = -20$–20 mm and $y = 0$–10 mm. The effect of the EHD force can be calculated by the rate of momentum change in the x direction:

$$F_x = \mathrm{d}M_x/\mathrm{d}t. \tag{3}$$

According to the PIV diagrams, momentum in the x direction can be calculated by the integral of the horizontal velocity profile in the control body:

$$M_x = \rho \int_A U \mathrm{d}A. \tag{4}$$

where the dimension of momentum is kg·m/s or N·s (1 N = 1 kg·m/s^2).

Momentum has significant impact on the actuator's capability to induce the EHD force. By selecting an appropriate control body in the fixed area of the induced flow field, and integrating the horizontal velocity profile, the x-directional induced momentum M_x in the fixed control body can be obtained, where $M_x = \int_A V \mathrm{d}A$ in units of N·s. Meanwhile, the change rate of momentum in the control body also reflects the change of the EHD force ($F_x = \mathrm{d}M_x/\mathrm{d}t$), which is the efficiency evaluation method of the plasma actuator that is widely used at present.[39]

The range of the control body is $x = -30$–0 mm, and $x = 0$–30 mm horizontally, and $y = 0$–10 mm vertically. M_x in DBD and extended discharge both appear at $T^* = 0.15$, and then momentum slowly declines. The peak of M_x in extended

discharge appears near $T^* = 0.3$, and M_x in extended discharge ($M_{x,\mathrm{EX-DBD}} = 1.96 \times 10^{-4}$ N·s) is higher than that in sliding discharge ($M_{x,\mathrm{SL-DBD}} = 1.78 \times 10^{-4}$ N·s), and the results are much higher than that in DBD ($M_{x,\mathrm{DBD}} = 0.69 \times 10^{-4}$ N·s). Momentum growth is the interaction of plasma actuation and air damping. Under the driving effect of plasma, the starting vortex accelerates. When there is no plasma any longer, the induced flow field is mainly affected by air damping, and the momentum decreases. According to Figs. 12 and 13, the maximum value and the vertical height of the velocity profile induced by extended discharge is high. In the same pulsed cycle, the momentum growth has a larger peak value and a faster growth rate. However, the momentum growth in sliding discharge lasts longer in the whole pulsed cycle, indicating that sliding discharge can also inject more momentum into the surrounding flow field. Bayoda *et al.*[28] observed the propagation of the ionization channels over the surface of the actuator, and the ionized channels of sliding discharge expand further. These measurements by phase provide the basis for the continuous momentum growth of sliding discharge.

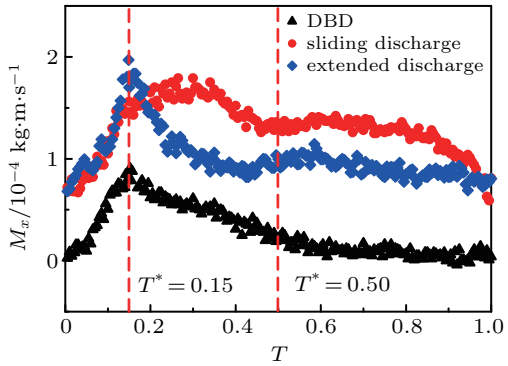


Fig. 15. Momentum change under different discharge modes within a period of $0.4T$.

Extended discharge has a higher effect on the velocity profile than the other two kinds of actuation, and sliding discharge has the characteristics of producing large-area plasma. With the comprehensive consideration, it can be known that both extended discharge and sliding discharge can generate strong aerodynamic efficiency above the surface of the actuator.

4. Conclusion

The high-frequency PIV system and high-speed schlieren system have been used to research the evolution of the flow field induced by extended discharge and sliding discharge of DSDPA. The following conclusions are obtained.

(1) Sliding discharge and extended discharge are filamentary discharge. During sliding discharge occurs, the irregular current pulses fluctuate significantly, and the discharge pulses have extremely high pulse peaks. The negative DC voltage accelerates the drift of the positive ions, ultimately forming the discharge channel having a width of 18 mm filled with high energy discharge filaments. Under the action of positive DC voltage, no stable sliding discharge zone can be formed in the electrode interval due to fact that positive ions play a major role in the charge drift. The instantaneous power and average power consumption of sliding discharge are larger than those of extended discharge and DBD.

(2) Sliding discharge induce the opposite jet at the side of the bias electrode. The opposite jet moves towards the starting vortex and the collision causes the movement direction of the flow field to deflect. Secondly, a bulge structure caused by the opposite jet is formed in the area of sliding discharge. In general, the existence of the bias electrode can change the direction of the flow field. It is helpful for DSDPA to apply directional disturbance to the external flow field.

(3) Extended discharge can accelerate the horizontal velocity profile of the starting vortex by increasing the induced velocity up to 203%. Extended discharge has the ability of accelerating the velocity profile. The maximum value and the vertical height of the velocity profile induced by extended discharge increase.

(4) In the same pulsed cycle, the momentum growth caused by extended discharge has a larger peak value and a faster growth rate. Extended discharge has a higher effect on the velocity profile than the other two kinds of actuation. However, the momentum growth of sliding discharge lasts longer in the whole pulsed cycle, indicating that sliding discharge can also inject more momentum into the surrounding flow field. Both extended discharge and sliding discharge can generate strong aerodynamic efficiency above the surface of DSDPA.

References

[1] Corke T C, Enloe C L and Wilkinson S P 2010 *Annu. Rev. Fliud Mech.* **42** 505
[2] Roth J R, Sherman D M and Wilkinson S P 1998 *36th AIAA Aerospace Sciences Meeting and Exhibit*, January 12–15, 1998, Reno, NV, USA p. 328
[3] Roth J R 2003 *Phys. Plasmas* **10** 2117
[4] Moreau E, Léger L and Touchard G 2006 *J. Electrostat.* **64** 215
[5] Roupassov D V, Nikipelov A A, Nudnova M M and Starikovskii A Y 2009 *AIAA J.* **47** 168
[6] Chen K and Liang H 2016 *Chin. Phys. B* **25** 024703
[7] Huang J, Corke T C, Thomas F O and Thomas F O 2006 *AIAA J.* **44** 51
[8] He C, Corke T C and Patel M P 2009 *J. Aircraft* **46** 864
[9] Patel M P, Ng T T, Vasudevan S, Corke T C and He C 2007 *J. Aircraft* **44** 1264
[10] Little J, Nishihara M, Adamovich I and Samimy M 2010 *Exp. Fluids* **48** 521
[11] Wei B, Wu Y, Liang H, Zhu Y F, Chen J, Zhao G Y, Song H M, Jia M and Xu H J 2019 *Int. J. Heat Mass Transfer* **138** 163
[12] Pavon S, Dorier J L, Hollenstein C, Ott P and Leyland P 2007 *J. Phys. D: Appl. Phys.* **40** 1733
[13] Shen L, Wen C Y and Chen H A 2016 *AIAA J.* **54** 652
[14] Pons J, Moreau E and Touchard G 2005 *J. Phys. D: Appl. Phys. J.* **38** 3635
[15] Moreau E, Sosa R and Artana G 2008 *J. Phys. D: Appl. Phys.* **41** 115204
[16] Zheng B R, Xue M, Ke X Z, Ge C, Wang Y S, Liu F and Luo S J 2019 *AIAA J.* **57** 467

[17] Seney S, Huffman R, Bailey W, Liu D, Reeder M and Stults J 2011 *42nd AIAA Plasmadynamics and Lasers Conference in Conjunction with the 18th International Conference on MHD Energy Conversion (ICMHD)* June 27–30, 2011, Honolulu, Hawaii, USA, p. 3732
[18] Moreau E, Louste C and Touchard G 2008 *J. Electrostat.* **66** 107
[19] Benard N and Moreau E 2014 *Exp. Fluids* **55** 1846
[20] Steven D S, Richard E H, William B, Liu D, Reeder M F and Stults J 2016 *AIAA J.* **54** 10
[21] Zheng B R, Xue M and Ge C 2020 *Chin. Phys. B* **29** 064703
[22] Louste C, Artana G, Moreau E and Touchard G 2005 *J. Electrostat.* **63** 615
[23] Moreau E, Sosa R and Artana G 2008 *J. Phys. D: Appl. Phys.* **41** 115
[24] Guo S, Simon T, Ernie D and Kortshagen U 2010 *48th AIAA Aerospace Sciences Meeting Including the New Horizons Forum and Aerospace Exposition*, January 4–7, 2010, Orlando, Florida, USA, p 1090
[25] Zheng B R, Ke X Z, Ge C, Zhu Y F, Wu Y, Liu F and Luo S J 2020 *AIAA J.* **58** 733
[26] Pang L, He K, Zhang Q G and Liu C L 2016 *Phys. Plasmas* **23** 053513
[27] Pang L, He K and Zhang Q G 2016 *J. Appl. Phys.* **120** 103302
[28] Bayoda K D, Benard N and Moreau E 2015 *J. Appl. Phys.* **118** 063301
[29] Kong F, Wang Y, Zhang C, Che X K, Yan P and Shao T 2017 *Phys. Plasmas* **24** 123503
[30] Zhang C, Huang B D, Luo Z B, Che X K, Yan P and Shao T 2019 *Plasma Sources Sci. Technol.* **28** 064001
[31] Fang Z, Qiu Y, Zhang C and Kuffel E 2007 *J. Phys. D: Appl. Phys.* **40** 1401
[32] Soloviev V R and Krivtsov V M 2009 *J. Phys. D: Appl. Phys.* **42** 125208
[33] Xie X Q, Fang Z, Yang H, Qiu Z, Zhao L Z and Qiu Y C 2009 *Chin. J. Vac. Sci. Technol.* **29** 649 (in Chinese)
[34] Jiang X 2017 *Characteristics and Application Research on a Sliding Discharge Plasma Actuator* (MS thesis) (Nanjing: Nanjing University of Aeronautics and Astronautics) (in Chinese)
[35] Zheng B R, Xue M and Ge C 2020 *Chin. Phys. B* **29** 024704
[36] Soloviev V R 2012 *J. Phys. D: Appl. Phys.* **45** 025205
[37] Nishida H, Nakai K and Matsuno T 2017 *AIAA J.* **55** 1852
[38] Nakai K, Hasegawa D, Hatamoto A and Nishida H 2019 *AIAA Scitech Forum*, January 7–11, 2019, San Diego, California, USA, p. 0737
[39] Jukes T N and Choi K S 2009 *Phys. Fluids* **21** 094106